Nonresonant hydrogen dopants in In(AsN): A route to high electron concentrations and mobilities

N. V. Kozlova,[1,2] G. Pettinari,[1] O. Makarovsky,[1] N. Mori,[3] A. Polimeni,[4] M. Capizzi,[4] Q. D. Zhuang,[5] A. Krier,[5] and A. Patanè[1,*]

[1]*School of Physics and Astronomy, The University of Nottingham, Nottingham NG7 2RD, UK*
[2]*IFW Dresden, Institute for Metallic Materials, P.O. Box 270116, Dresden D-01171, Germany*
[3]*Graduate School of Engineering, Osaka University, 2-1 Yamada-Oka, Suita City, Osaka 565-0871, Japan*
[4]*Dipartimento di Fisica, Sapienza Università di Roma, Piazzale A. Moro 2, 00185 Roma, Italy*
[5]*Physics Department, Lancaster University, Lancaster LA1 4YB, UK*

(Received 21 December 2012; revised manuscript received 4 April 2013; published 23 April 2013)

We provide evidence for the unique effect of hydrogen on the transport properties of the mid-infrared alloy In(AsN). High electron concentrations and mobilities are simultaneously achieved in hydrogenated In(AsN), and Shubnikov-de Haas oscillations are observed up to near room temperature. These results can be accounted for by the formation of N-H donor complexes with energy levels well above the Fermi energy, far from resonance with the conduction electrons, thus resulting in weak electron scattering even at high donor concentrations. Similar effects should be found in other narrow band gap dilute nitride alloys.

DOI: 10.1103/PhysRevB.87.165207 PACS number(s): 72.80.Ey, 73.20.Hb, 73.43.Qt, 75.47.−m

I. INTRODUCTION

Semiconductor doping, during or after growth, underpins modern devices and technologies because it permits accurate control of the free-carrier concentration.[1] On the other hand, the ensuing impurity scattering degrades the carrier mobility and limits the performance of devices based on highly doped semiconductors. This drawback can be partially overcome by modulation doping, i.e., by doping semiconductor regions that are spatially separated from the conducting channel,[2] thus resulting in a significant reduction of carrier scattering by charged impurities, even at low temperatures. Whenever modulation doping cannot be implemented, alternative routes should be considered. This is not a trivial task for material systems with unconventional electronic properties, such as dilute nitride III-N-V alloys.[3] In III-N-Vs, the behavior of both n- and p-type impurities is influenced by the highly electronegative nitrogen atoms and can be significantly different from that reported for III-V compounds.[4–7] In particular, nitrogen-related complexes can introduce localized states above the conduction band minimum (CBM) of the host III-V crystal. Since the nitrogen central-cell potential is large (∼7 eV), the electron scattering rate is resonantly enhanced at the energy of these states.[8,9] This phenomenon differs from long-range Coulomb scattering by ionized impurities, which gives a monotonic decrease of the scattering rate with increasing electron energy[10] and dominates over inelastic collisions by phonons even at room temperature.[9]

In this paper, we demonstrate that the electron density in the dilute nitride alloy In(AsN) can increase upon hydrogen incorporation by two orders of magnitude without an increase of the electron scattering rate. High electron concentrations (up to 10^{19} cm^{-3}) and mobilities ($>10^3$ cm^2 V^{-1} s^{-1}) are simultaneously achieved in In(AsN), and Shubnikov-de Haas (SdH) oscillations are observed up to near room temperature. The conductivity enhancement is attributed to the formation of N-H complexes with donor states well above the electron Fermi energy, far from resonance with the conduction electrons. Thus, the central-cell potential of the complexes has no pronounced effects on the conduction, resulting in an effective modulation doping in energy-space in which electrons and donors are separated in energy rather than in real space. This study has broad implications for research and future applications in fast electronics and mid-infrared photonics of compounds, such as In(AsN), In(AsSbN), In(SbN), etc., to which this doping concept could be effectively extended.

II. SAMPLES AND EXPERIMENT

The In(AsN) epilayers (thickness $t = 0.8$–1.5 μm and nitrogen content [N] = 0.0, 0.2, 0.4, and 1%) were grown by molecular beam epitaxy on semi-insulating (100)-oriented GaAs substrates. Despite the presence of misfit and threading dislocations in all these layers, our optical studies indicate that In(AsN) grown onto GaAs exhibits little or no degradation of the photoluminescence properties compared with epitaxial layers grown on InAs, and that in both structures (i.e., In(AsN) on GaAs and InAs) the incorporation of nitrogen leads to comparable red shifts of the fundamental band gap.[11] Also, in stark contrast to other dilute nitride alloys, such as Ga(AsN), the electrical conductivity retains the characteristic features of transport through extended states with electron mobilities that remain relatively large even for [N] = 1% ($\mu_e = 6 \times 10^3$ cm^2 V^{-1} s^{-1} at 300 K).[12]

All wafers were processed into Hall bars of length $L = 1250$ μm and width $W = 250$ μm. Metal contacts consisting of 10 nm of Ti followed by 200 nm of Au were deposited onto the samples to provide ohmic contacts. Hydrogen was implanted in the epilayers at a temperature $T = 250$ °C using a Kaufman source with an ion-beam energy of 100 eV for 1 and 6 hours and impinging H-doses $d_H = 4 \times 10^{17}$ ions/cm^2 (dose H) and $d_H = 10^{19}$ ions/cm^2 (dose 25H). For the magnetotransport studies, the magnetic field was applied parallel to the growth axis z, i.e., $\boldsymbol{B} = [0, 0, B_z]$, or at an angle θ relative to z (see the top inset of Fig. 1). The transverse magnetoresistance ratio, defined as $\Delta R_{xx}/R_{xx} = [R_{xx}(B) - R_{xx}(0)]/R_{xx}(0)$, was measured in pulsed magnetic fields up to 50 T (total pulse length of 100 ms) or in static fields up to 14 T. The experimental set-up for micro-Raman measurements comprises an optical

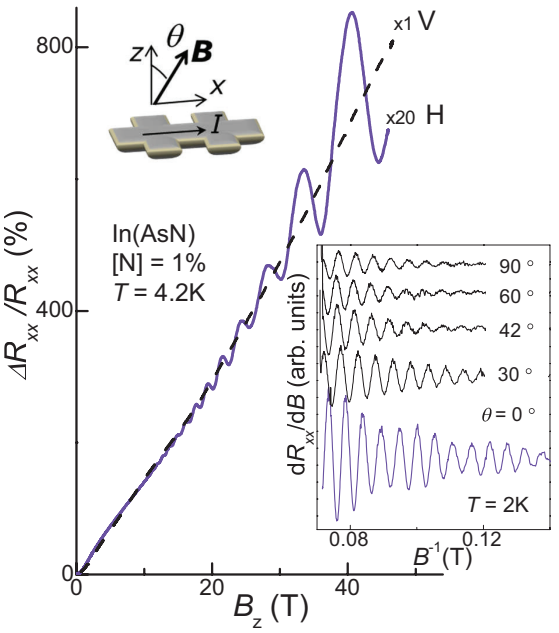

FIG. 1. (Color online) Low temperature ($T = 4.2$ K) transverse magnetoresistance, $\Delta R_{xx}/R_{xx}$, versus magnetic field, B_z, for an In(AsN) Hall bar with [N] = 1% before (V) and after (H) hydrogenation ($d_{\rm H} = 4 \times 10^{17}$ ions/cm^2). The top inset sketches a Hall bar and the angle θ between $\boldsymbol{B}$ and the z axis. The right inset shows dR_{xx}/dB versus B^{-1} for $\boldsymbol{B}$ tilted at different angles θ ($T = 2$ K).

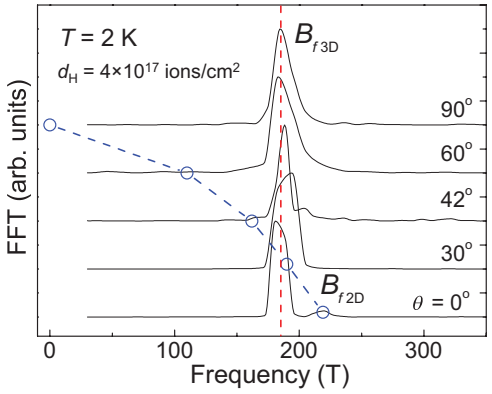

FIG. 2. (Color online) Fast Fourier Transform (FFT) analysis of the SdH oscillations in the resistance (R_{xx}) for different angles θ of magnetic field $\boldsymbol{B}$ for an In(AsN) Hall bar with [N] = 1% and $d_{\rm H} = 4 \times 10^{17}$ ions/cm^2 ($T = 2$ K). For $\theta = 0°$, two peaks are observed at frequencies $B_{f3D} = (185 \pm 5)$ T and $B_{f2D} = (230 \pm 5)$ T. B_{f3D} is independent of θ (see vertical line), thus indicating that is associated with the SdH effect in a 3D electron gas of density $n_e = (2eB_{f3D}/\hbar)^{3/2}/(3\pi^2) = 1.4 \times 10^{19}$ cm^{-3}. The peak at B_{f2D} is clearly observed only for $\theta = 0°$ and originates from the SdH effect in a 2D surface accumulation layer with electron density $n_e = 2eB_{f2D}/h = 1.1 \times 10^{13}$ cm^{-2}. For a 2D surface accumulation, this peak should shift at lower frequency for increasing θ according to $B_{f2D} \sim \cos(\theta)$ (see blue line and symbols).

confocal microscope equipped with a nano-focusing system, a spectrometer with a 1200 g/mm grating, and a charge-coupled device. For the excitation, we used an He-Ne laser with $\lambda = 633$ nm. The laser beam was focused to a diameter $d \sim 1$ μm using a 100 $\times$ objective.

III. RESULTS AND DISCUSSION

A. H-induced increase of the electron density in In(AsN)

Figure 1 shows the B_z dependence of $\Delta R_{xx}/R_{xx}$ at $T = 4.2$ K for an In(AsN) Hall bar with [N] = 1% before and after the hydrogenation with dose H ($d_{\rm H} = 4 \times 10^{17}$ ions/cm^2). The virgin sample (V) shows a positive linear magnetoresistance at $B_z > 1$ T. Following the hydrogenation, the strength of linear magnetoresistance is reduced by a factor of 20, and SdH oscillations emerge at $B_z > 5$ T. As can be seen in the right inset, the magneto-oscillations are observed for $\boldsymbol{B}$ tilted at various angles from $\theta = 0°$ to 90°. The positions in $1/B$ of the maxima/minima in dR_{xx}/dB do not scale as $1/B\cos\theta$, thus indicating that they are caused by the SdH effect in a three-dimensional (3D) electron gas. Also, a Fourier analysis of the SdH oscillations reveals a beating pattern at $\theta = 0°$, which disappears at larger θ (see Fig. 2). This is attributed to a weak contribution from SdH oscillations in a two-dimensional (2D) accumulation layer forming at the sample surface and due to the pinning of the Fermi level by extrinsic (hydrogen) and intrinsic donorlike surface states.[13,14]

The oscillatory component of R_{xx}, which quenches slowly with increasing temperature, can be observed up to high temperature ($T = 270$ K) (see the top inset of Fig. 3), whereas the strength of linear magnetoresistance and the value of R_{xx} change only weakly (see Fig. 3). The period $B_f^{-1} = \Delta(1/B_z) = (0.0054 \pm 0.0002)\ T^{-1}$ in the maxima/minima

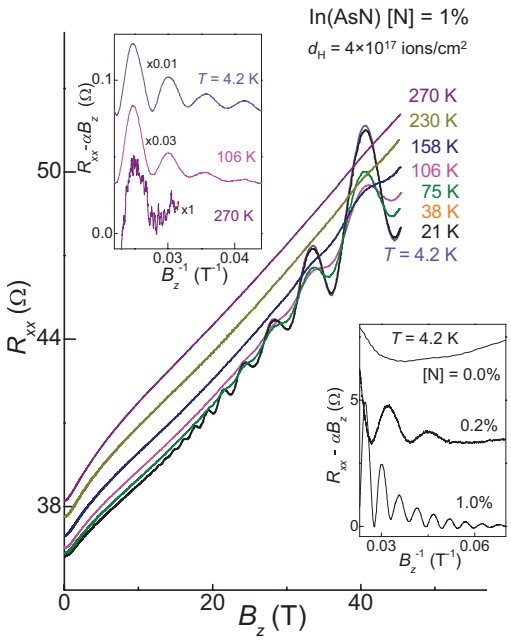

FIG. 3. (Color online) Temperature dependence of the resistance R_{xx} versus magnetic field (B_z) for a hydrogenated In(AsN) Hall bar with [N] = 1% ($d_{\rm H} = 4 \times 10^{17}$ ions/cm^2). To reveal the oscillatory peaks in R_{xx}, in the top inset we plot the dependence of R_{xx}-αB_z on $B_z{}^{-1}$ (where α is a constant) at different temperatures. The dependence of R_{xx}-αB_z on $B_z{}^{-1}$ is also shown on the bottom inset at fixed temperature ($T = 4.2$ K) for hydrogenated In(AsN) Hall bars with [N] = 0%, 0.2%, and 1% and $d_{\rm H} = 4 \times 10^{17}$ ions/cm^2.

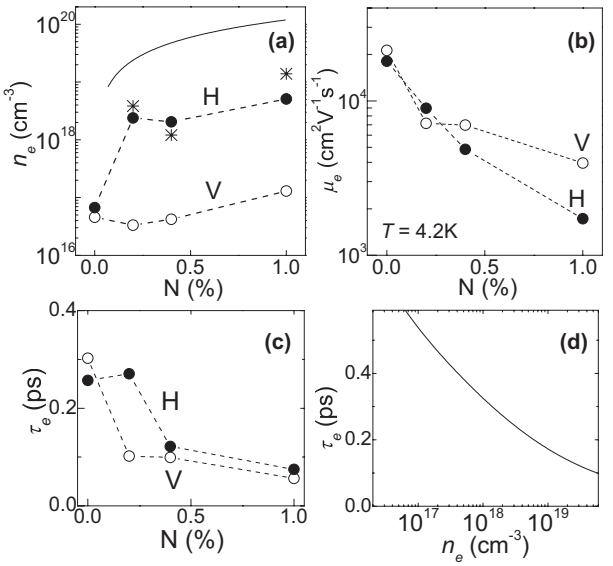

FIG. 4. (a) and (b) Dependence of the electron density (n_e) and mobility (μ_e) on [N] before (V) and after (H) hydrogenation ($d_H = 4 \times 10^{17}$ ions/cm^2) at $T = 4.2$ K. The values of n_e are derived from the analysis of the Shubnikov-de Haas oscillations (asterisks) and the Hall resistance (dots and circles). Dotted lines are guides to the eye. The continuous line in (a) shows the density of N atoms. (c) Dependence of the electron scattering time (τ_e) on [N] as derived from $\tau_e = \mu_e m_e^*/e$ before (V) and after (H) hydrogenation ($d_H = 4 \times 10^{17}$ ions/cm^2) at $T = 4.2$ K. (d) Calculated dependence of τ_e on the electron density n_e according to the Brooks-Herring model.

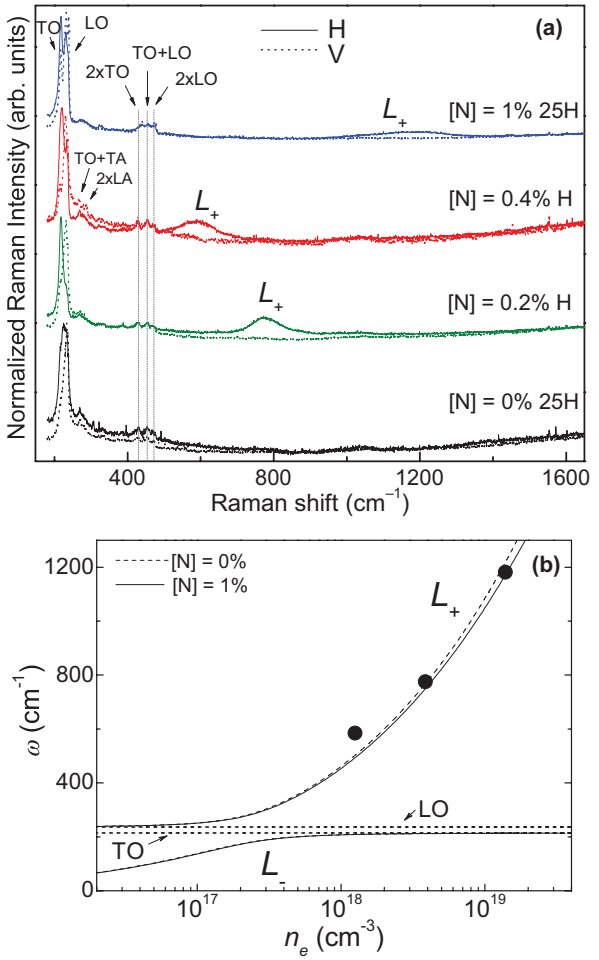

FIG. 5. (Color online) (a) Normalized micro-Raman spectra of In(AsN) epilayers before (dotted lines) and after (solid lines) hydrogen incorporation. The spectra were acquired at $T = 300$ K with a laser of power density $P \sim 10^5$ W/cm^2, wavelength $\lambda = 633$ nm, and spot diameter $d \sim 1$ μm. The H dose (H: 4×10^{17} ions/cm^2 and 25H: 10^{19} ions/cm^2) is indicated in the figure for each epilayer. (b) Calculated dependence of the frequencies $\omega_\pm$ of the coupled LO phonon-plasmon modes, L_+ and L_-, on the electron density n_e for [N] = 0% (dashed line) and [N] = 1% (continuous line). The horizontal lines represent the values of the measured frequencies of the TO and LO modes in InAs. Symbols correspond to the measured values of ω_+ in hydrogenated In(AsN).

of R_{xx} at $\theta = 0^\circ$ and $T = 4.2$ K gives a 3D electron density $n_e = (2e/\hbar\Delta)^{3/2}/(3\pi^2) = (1.4 \pm 0.1) \times 10^{19}$ cm^{-3}. B_f^{-1} and n_e depend only weakly on temperature in the range 4.2–270 K. Also, n_e does not increase further after a second hydrogenation with a 25 times larger dose ($d_H = 10^{19}$ ions/cm^2), and its values are close to those derived from the analysis of the Hall resistance, R_{xy}, i.e., $n_e = B_z/(eR_{xy}d) = 0.5 \times 10^{19}$ cm^{-3} (dose H) and $n_e = 1.2 \times 10^{19}$ cm^{-3} (dose 25H) at $T =$ 4.2-290 K, where the effective thickness of the conducting channel, d, has been assumed equal to the nominal thickness of the In(AsN) epilayer ($t = 1.3$ μm). Thus, the discrepancy between the values of n_e derived from the period of the SdH oscillations and the Hall-resistance R_{xy} indicates that $d \leqslant t$ and that, under appropriate hydrogenation conditions, a uniform electron density across the epilayer is achieved.

The electron Hall density in the hydrogenated In(AsN) sample with [N] = 1% ($n_e \sim 10^{19}$ cm^{-3}) is almost two orders of magnitude higher than in the virgin epilayer ($n_e = 1.3 \times 10^{17}$ cm^{-3}). As shown in Fig. 4(a), In(AsN) samples with [N] = 0.2% and 0.4% show a similar large increase of n_e. In contrast, in the InAs Hall bar, the electron density changes only from $n_e = 5 \times 10^{16}$ cm^{-3} to 7×10^{16} cm^{-3} and 16×10^{16} cm^{-3} upon the H- and 25H-hydrogenations, respectively; SdH oscillations are not observed in this case (see the bottom inset of Fig. 3). This hydrogen-induced increase of the electron density in the In(AsN) epilayers with N > 0% is confirmed by the observation of coupled longitudinal optical (LO) phonon-plasmon modes in the micro-Raman scattering spectra. Figure 5(a) shows the normalized micro-Raman spectra of In(AsN) epilayers before (dotted lines) and after (solid lines) hydrogen incorporation. The Raman peaks associated with the transverse optical (TO), LO phonons, and their Raman second order, dominate the spectra at low frequency ($\leqslant$500 cm^{-1}). Weaker peaks associated with acoustic modes are also visible in the 260–300 cm^{-1} frequency range.[15] Following the hydrogenation, a broad peak, L^+, emerges at high frequencies in the N-containing epilayers. The L^+ line is attributed to a coupled LO phonon-plasmon mode. The dependence of the L^+ frequency on the electron density will be discussed later.

For the hydrogenated InAs Hall bar, the small increase of n_e suggests a donor behavior of hydrogen, which is similar to that reported in the literature for n-type InAs[16] and other compounds with a low CBM relative to the vacuum (e.g., ZnO

and InN).[17,18] The much larger increase of n_e in hydrogenated In(AsN) should be accounted for instead by a greater tendency of hydrogen to create donors by forming bonds with the strongly electronegative N atoms. The existence of a H-N donor has been predicted for Ga(AsN)[5] but never reported experimentally. In Ga(AsN), the lowest energy configuration for single H corresponds to a bond-center site next to nitrogen, $H(BC_N)$.[5] This phenomenology should hold in In(AsN), too, but with an important difference in the energy position of the $H(BC_N)$ donor level, $E_{H\text{-}N}$, which is caused by the larger electron affinity of InAs ($\chi = 4.9$ eV) compared to GaAs ($\chi = 4.1$ eV). For [N] = 1%, we estimate that $E_{H\text{-}N}$ should be at least ~0.8 eV above the CBM of In(AsN),[19–21] much higher than in Ga(AsN), where it is expected to be nearer to the CBM.[5] Thus resonant scattering of electrons by the central-cell potential of $H(BC_N)$ should not be significant in In(AsN). In fact, the electron mobility does not decrease significantly after the hydrogenation ($\mu_e > 10^3$ cm^2 V^{-1} s^{-1} at 4.2 K), as shown in Fig. 4(b) for different [N] concentrations. Also, as discussed below, the hydrogen-induced small decrease of μ_e for [N] = 1% is caused by the larger effective mass at the Fermi energy that electrons have for high n_e values (~10^{19} cm^{-3}) in the nonparabolic conduction band of In(AsN) rather than to electron scattering by the ionized donors. Finally, we note that hydrogen configurations other than the $H(BC_N)$ donors could become energetically more favorable at high electron densities,[5] thus explaining the measured saturation of n_e to about 10% of the total N concentration for increasing H doses, see Fig. 4(a).

B. Electron mass, mobility, and scattering time

We examine now the effects of hydrogen on the scattering time. We compare the measured values of the electron mass and density, as derived from the analysis of the SdH oscillations and their temperature dependence,[22] with those calculated using a simple model. The electron energy dispersion of InAs is modeled as $\varepsilon(\boldsymbol{k})[1 + \alpha\varepsilon(\boldsymbol{k})] = \hbar^2k^2/2m_0^*$,[10,23] where $\alpha = 2$ eV^{-1}, $m_0^* = 0.025\, m_e$ is the electron effective mass at $\boldsymbol{k} = 0$, and m_e is the electron mass in vacuum. In In(AsN), the energy dispersion is modified by the interaction of the N level with the CB states, described here by a two-level band-anticrossing model with an interaction parameter $V_N =$ 2.0 eV and a N level at 1.44 eV above the valence band of InAs.[18–20] As shown in Fig. 6(a), the calculated dependence of the first derivative electron mass, $m_e^* = \hbar^2k/[d\varepsilon/dk]$, on $n_e = k^3/3\pi^2$ does not change significantly for [N] ranging from 0% (dashed line) to 1% (continuous line). Also, it matches well the measured values of m_e^* versus n_e (full symbols). Since SdH oscillations are not resolved before hydrogenation, in Fig. 6(a) we plot also the values of the electron cyclotron resonance (CR) mass (empty symbols) reported previously[24] for as-grown In(AsN) with excitation photon wavelengths $\lambda = 103.0\ \mu$m and 66.0 μm.[25]

The measured frequency ω_+ of the LO phonon-plasmon coupled L_+ mode is also well described by this model. In a polar semiconductor, the coupling between the LO modes and the collective excitations of the free-carrier plasma gas (plasmons) results in two coupled phonon-plasmon modes $L_\pm$ of frequency $\omega_\pm$ given by $2\omega_\pm^2 = \omega_p^2 + \omega_{LO}^2 \pm \sqrt{(\omega_p^2 + \omega_{LO}^2)^2 - 4\omega_p^2\omega_{TO}^2}$.[26] Here ω_{LO} and ω_{TO} are the frequencies of the LO and TO modes, and ω_p is the plasma frequency. The latter depends on the electron density (n_e) and electron effective mass (m_e^*) according to $\omega_p^2 = (n_e e^2)/(\kappa_0\kappa_r m_e^*)$. To calculate $\omega_\pm$, we use the measured Raman shifts of the TO (214.3 cm^{-1}) and LO (236.7 cm^{-1}) modes, the dielectric constant $\kappa_r = 12$, and the calculated dependence of m_e^* on n_e for InAs and In(AsN) with [N] = 1%. As shown in Fig. 5(b), the calculated dependences of $\omega_\pm$ on n_e are similar in InAs (dashed line) and In(AsN) (continuous line), and describe well the frequency of the L_+ mode as measured in the hydrogenated In(AsN) epilayers. The Raman data and analysis provide an independent confirmation that hydrogen increases significantly the electron concentration in the In(AsN) alloy.

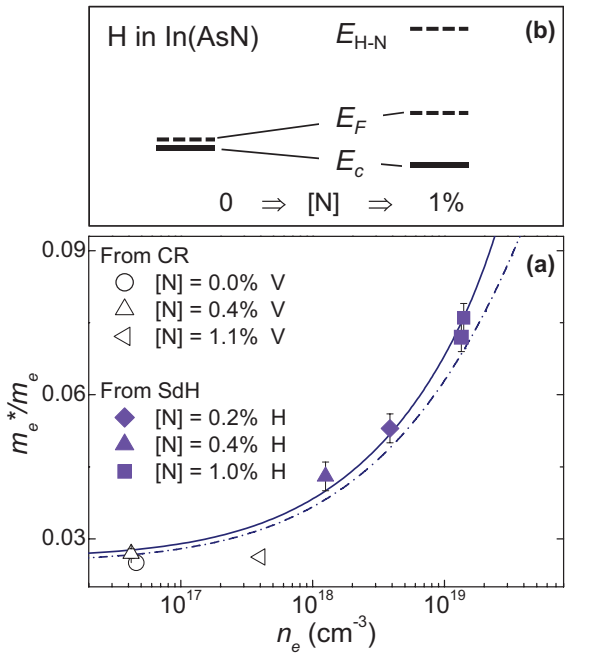

FIG. 6. (Color online) (a) Calculated (lines) and measured (symbols) dependences of the first derivative electron mass (m_e^*) on the electron density (n_e). Dashed and continuous lines correspond to InAs and In(AsN) ([N] = 1%), respectively. Empty symbols correspond to values of m_e^* derived from cyclotron resonance studies of virgin samples (see Ref. 25). Full symbols correspond to values of m_e^* derived from the T dependence of the Shubnikov-de Haas oscillations. (b) Conduction band minimum (E_C), Fermi energy (E_F), and energy level ($E_{H\text{-}N}$) of the H-N donor complex. $E_F - E_C =$ 0.29 eV and 0.02 eV for [N] = 1% and 0%, respectively.

In the In(AsN) sample with [N] = 1%, m_e^* increases upon hydrogenation by a factor of 2.5 for an increase of n_e by a factor ~100 from 1.3×10^{17} cm^{-3} to 1.4×10^{19} cm^{-3} [see Fig. 6(a)]. This increase accounts for the corresponding 2.4 reduction in the electron mobility, μ_e, from 4×10^3 cm^2 V^{-1} s^{-1} to 1.7×10^3 cm^2 V^{-1} s^{-1} at $T = 4.2$ K, thus indicating that the electron scattering time $\tau_e = \mu_e m_e^*/e$ does not change sizably upon the hydrogen-induced increase of n_e. Figure 4(c) shows the values of τ_e as obtained from this analysis for all samples. Note that for [N] > 0%, the electron scattering time increases slightly after hydrogenation, even in the sample with [N] = 1%, in spite of an increase

by two orders of magnitude in the electron (and donor) concentration. For this In(AsN) epilayer, the Fermi energy $[E_F = \hbar e B m_e^{*-1}(N_{LL} + 1/2)]$ is 0.29 eV above the CBM, much lower than the energy level of $H(BC_N)$ (>0.8 eV above CBM, as estimated from Ref. 5), see Fig. 6(b).[27]

Since the energy of the $H(BC_N)$ donor is far from resonance with the conduction electrons, the central-cell potential of the complex does not cause a significant scattering. To estimate the contribution to the scattering time of long-ranged Coulomb scattering by the positively charged dopants, we consider the Brooks-Herring formula within a two-band model.[10,23,28] The scattering time τ_e at the Fermi energy is calculated using the relation

$$\tau_e(E_F) = 16\pi\kappa^2 e^{-4} n_I^{-1} \sqrt{2m_0^*}(1 + 2\alpha E_F)^{-1} \times [E_F(1 + \alpha E_F)]^{3/2} F(\xi)^{-1}, \quad (1)$$

where $n_I = n_e$ is the density of ionized impurities, $\kappa = \kappa_r \kappa_0$ is the dielectric constant ($\kappa_r = 15$), $F(\xi) = \ln(1 + \xi) - \xi(1 + \xi)^{-1}$, $\xi = (2k/q_s)^2$, $q_s = \sqrt{e^2\kappa^{-1} g(E_F)}$ is the inverse of the screening length at $T = 0$ K and

$$g(E_F) = \frac{1}{2\pi^2}\left(\frac{2m_0^*}{\hbar^2}\right)^{3/2}(1 + 2\alpha E_F)\sqrt{E_F(1 + \alpha E_F)} \quad (2)$$

is the density of states at the Fermi energy.[28] We find that τ_e decreases from 0.5 ps to 0.2 ps with n_e increasing from 10^{17} cm^{-3} to 10^{19} cm^{-3} [see Fig. 4(d)]. The calculated values of τ_e are comparable to those derived from $\tau_e = \mu_e m_e^*/e$ for both the hydrogenated and virgin In(AsN) epilayers, thus indicating that electron scattering is not limited by the long-range Coulomb potential of the donors.

Finally, we examine an additional effect of the hydrogen incorporation on the magnetotransport properties of these In(AsN) epilayers. As illustrated in Figs. 1 and 3, a linear magnetoresistance is observed in the In(AsN) virgin layer and is reduced by a factor of 20 after the hydrogenation. Linear magnetoresistance has been observed previously in many material systems and can originate from distortions in the current path induced by disorder.[29,30] Monte Carlo simulations of the electron dynamics have revealed that linear magnetoresistance can arise from multiple scattering of the current-carrying electrons by low-mobility islands within the conducting layer.[29] Since our InAs and In(AsN) epilayers are grown on highly lattice-mismatched GaAs, threading dislocations tend to form at the epilayer/substrate interface[11] and are likely to cause local macroscopic (> 0.1 μm) variations in the electron mobility. In particular, the strength of the linear magnetoresistance depends on the island-coverage factor f according to a simple relation, i.e., $\Delta R_{xx}/R_{xx} = 0.5 f(1 - f)^{-1}\mu_e B_z$.[30] From a linear fit to the measured data by this expression, we find that f decreases in all hydrogenated layers (from 30% to 10% for [N] = 1%). This suggests that hydrogen could lead to both the passivation of crystal defects in the vicinity of the low-mobility islands and a more uniform mobility and conduction along the Hall bar.

IV. CONCLUSIONS

In summary, H incorporation in the dilute nitride In(AsN) alloy induces a remarkable increase of n-type conductivity as well as SdH oscillations up to near room temperature, while it reduces the strength of linear magnetoresistance. These findings are attributed to the formation of N-H donor complexes with energy levels well above the Fermi energy, far from resonance with the conduction electrons. Thus, high electron concentrations and mobilities are simultaneously achieved in In(AsN), unlike other dilute nitride alloys where the conductivity is severely degraded by resonant scattering by deep levels in the conduction band. This study will stimulate theoretical studies of hydrogen levels in In(AsN) and other mid-infrared III-N-V alloys, where hydrogen can be an unintentional or intentional dopant, and also fuel research on modulation doping in energy space to increase free carrier density without degrading the carrier mobility.

ACKNOWLEDGMENTS

This work was supported by the EPSRC, DFG KO 3743/1-1, AOBJ: 550341, The Royal Society (RG110416), the COST Action MP0805, and the EU (under Grant No. PIEF-GA-2010-272612). We acknowledge N. Berdunov, M. De Luca, and L. Eaves for useful discussions.

*Corresponding author: amalia.patane@nottingham.ac.uk

[1] S. M. Sze, *Semiconductor Devices, Physics and Technology* (John Wiley & Son, New York, 2002).
[2] R. Dingle, H. L. Stormer, A. C. Gossard, and W. Wiegmann, Appl. Phys. Lett. **33**, 665 (1978).
[3] I. A. Buyanova and W. M. Chen, *Physics and Applications of Dilute Nitrides* (Taylor & Francis, New York, 2004).
[4] K. M. Yu, W. Walukiewicz, J. Wu, D. E. Mars, D. R. Charmberlin, M. A. Scarpulla, O. D. Dubon, and J. F. Geisz, Nat. Mater. **1**, 185 (2002).
[5] A. Janotti, S. B. Zhang, Su-Huai Wei, and C. G. Van de Walle, Phys. Rev. Lett. **89**, 086403 (2002).
[6] J. Li, P. Carrier, S. H. Wei, S. S. Li, and J. B. Xia, Phys. Rev. Lett. **96**, 035505 (2006).
[7] M.-H. Du, S. Limpijumnong, and S. B. Zhang, Phys. Rev. Lett. **97**, 075503 (2006).
[8] S. Fahy, A. Lindsay, H. Ouerdane, and E. P. O'Reilly, Phys. Rev. B **74**, 035203 (2006).
[9] O. F. Sankey, J. D. Dow, and K. Hess, Appl. Phys. Lett. **41**, 664 (1982).
[10] C. Hamaguchi, *Basic Semiconductor Physics* (Springer-Verlag, London, 2006).
[11] M. de la Mare, Q. Zhuang, A. Patanè, and A. Krier, J. Phys. D: Appl. Phys. **45**, 395103 (2012).
[12] A. Patanè, W. H. M. Feu, O. Makarovsky, O. Drachenko, L. Eaves, A. Krier, Q. D. Zhuang, M. Helm, M. Goiran, and G. Hill, Phys. Rev. B **80**, 115207 (2009).
[13] L. Ö. Olsson, C. B. M. Andersson, M. C. Håkansson, J. Kanski, L. Ilver, and U. O. Karlsson, Phys. Rev. Lett. **76**, 3626 (1996).
[14] J. R. Weber, A. Janotti, and C. G. Van de Walle, Appl. Phys. Lett. **97**, 192106 (2010).

[15]R. Carles, N. Saint-Cricq, J. B. Renucci, M. A. Renucci, and A. Zwick, Phys. Rev. B **22**, 4804 (1980).
[16]B. Theys, A. Lusson, J. Chevallier, C. Grattepain, and M. Stutzmann, J. Appl. Phys. **70**, 1461 (1991).
[17]C. G. Van de Walle and J. Neugebauer, Nature **423**, 627 (2003).
[18]A. Janotti and C. G. Van de Walle, Appl. Phys. Lett. **92**, 032104 (2008).
[19]I. Vurgaftman and J. R. Meyer, J. Appl. Phys. **94**, 3675 (2003).
[20]M. Merrick, S. A. Cripps, B. N. Murdin, T. J. C. Hosea, T. D. Veal, C. F. McConville, and M. Hopkinson, Phys. Rev. B **76**, 075209 (2007).
[21]J. Ibáñez, R. Oliva, M. De la Mare, M. Schmidbauer, S. Hernández, P. Pellegrino, D. J. Scurr, R. Cuscó, L. Artús, M. Shafi, R. H. Mari, M. Henini, Q. Zhuang, A. Godenir, and A. Krier, J. Appl. Phys. **108**, 103504 (2010).
[22]The electron mass m_e^* is derived from the temperature dependence of the amplitude A of the SdH oscillations, i.e., $A(T) = \chi/\sinh\chi$, where $\chi = 2\pi^2 k_B T m_e^*/(e\hbar)$.
[23]E. O. Kane, J. Phys. Chem. Solids **1**, 249 (1957).
[24]The temperature dependence of the SdH oscillations permits us to measure the electron mass, m_e^*, at the Fermi energy, while CR absorption in highly degenerate samples measures an electron mass averaged over a wide range of energies.
[25]O. Drachenko, A. Patanè, N. V. Kozlova, Q. D. Zhuang, A. Krier, L. Eaves, and M. Helm, Appl. Phys. Lett. **98**, 162109 (2011).
[26]E. D. Palik and J. K. Furdyna, Rep. Prog. Phys. **33**, 1193 (1970).
[27]m_e^* is the measured SdH electron mass, and N_{LL} is the Landau level associated with a given peak in $R_{xx}(B_z)$.
[28]W. Zawadzki and W. Szymansk, Phys. Status Solidi B **46**, 415 (1971).
[29]M. M. Parish and P. B. Littlewood, Nature **426**, 162 (2003).
[30]N. V. Kozlova, N. Mori, O. Makarovsky, L. Eaves, Q. D. Zhuang, A. Krier, and A. Patanè, Nature Commun. **3**, 1097 (2012).